Ⓔ

Strong-Motion Observations of the M 7.8 Gorkha, Nepal, Earthquake Sequence and Development of the N-SHAKE Strong-Motion Network

by Amod Mani Dixit, Adam T. Ringler, Danielle F. Sumy, Elizabeth S. Cochran, Susan E. Hough, Stacey S. Martin, Steven Gibbons, James H. Luetgert, John Galetzka, Surya Narayan Shrestha, Sudhir Rajaure, and Daniel E. McNamara

ABSTRACT

We present and describe strong-motion data observations from the 2015 **M** 7.8 Gorkha, Nepal, earthquake sequence collected using existing and new Quake-Catcher Network (QCN) and U.S. Geological Survey NetQuakes sensors located in the Kathmandu Valley. A comparison of QCN data with waveforms recorded by a conventional strong-motion (NetQuakes) instrument validates the QCN data. We present preliminary analysis of spectral accelerations, and peak ground acceleration and velocity for earthquakes up to **M** 7.3 from the QCN stations, as well as preliminary analysis of the mainshock recording from the NetQuakes station. We show that mainshock peak accelerations were lower than expected and conclude the Kathmandu Valley experienced a pervasively nonlinear response during the mainshock. Phase picks from the QCN and NetQuakes data are also used to improve aftershock locations. This study confirms the utility of QCN instruments to contribute to ground-motion investigations and aftershock response in regions where conventional instrumentation and open-access seismic data are limited. Initial pilot installations of QCN instruments in 2014 are now being expanded to create the Nepal–Shaking Hazard Assessment for Kathmandu and its Environment (N-SHAKE) network.

Online Material: Figures of *Pg* arrivals, earthquake locations, epicenter change vectors, and travel-time misfit vector residuals, and tables of QCN and NetQuake stations and relocated hypocenter timing, location, and magnitude.

INTRODUCTION

In spite of long-recognized high hazard along the Himalayan arc, strong-motion monitoring in Nepal has remained limited, and much of the existing data are not openly distributed (e.g., Nobuo *et al.*, 2015). For this reason, in 2014, the National Society for Earthquake Technology (NSET) installed a small number of Quake-Catcher Network (QCN; network code QC; see Data and Resources) Onavi-B 16-bit instruments as a pilot study to test the feasibility of using low-cost strong-motion sensors to improve monitoring in the Kathmandu Valley of Nepal. In general, QCN uses low-cost microelectromechanical systems (MEMS) accelerometers hosted by volunteers (Cochran *et al.*, 2009) to collect event records of moderate to large ground motions. In Nepal, local partners use sensors either internal to laptop computers, phones, or tablets or small (the size of a matchbox) MEMS Universal Serial Bus (USB) sensors (Cochran *et al.*, 2009) plugged into desktop computers and hosted by volunteers to collect scientifically useful seismic data. Data are collected and sent to a central server using the Berkeley Open Infrastructure for Network Computing distributed-computing software (Anderson and Kubiatowicz, 2002). Data from these instruments are freely available to the international community in near real time.

Three QCN stations were operational at the time of the 25 April 2015 **M** 7.8 Gorkha earthquake (Fig. 1); however, due to power failures, only the first few seconds of the mainshock were recorded at one station. Although a complete record of strong ground shaking is not available from QCN station 31523 (Fig. 1b), it was the nearest station, and the mainshock *P*-wave arrival was useful to improve the location of the hypocenter. After power was restored, the QCN instruments recorded early large aftershocks, including the **M** 7.3 aftershock on 12 May 2015. Data from these instruments are freely available to the international community in near real time. Five additional instruments were installed during a rapid aftershock mobilization program (RAMP) deployment in late May 2015, with an additional 30–40 instruments to be installed over the next year. The initial pilot installations and the additional

doi: 10.1785/0220150146

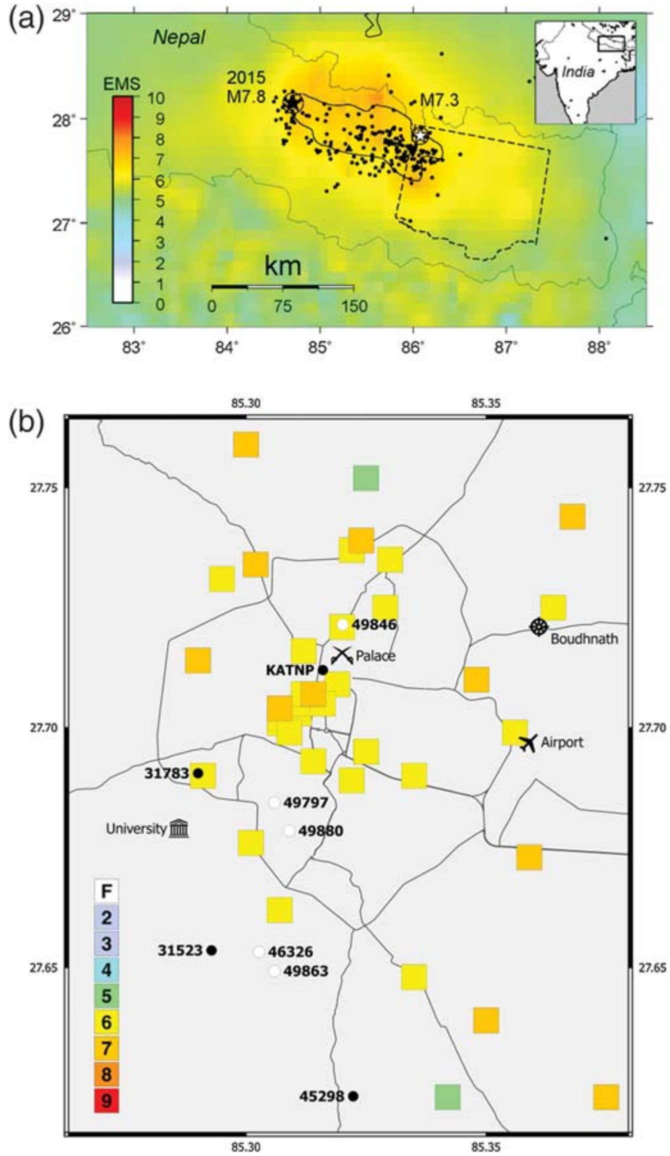

▲ **Figure 1.** (a) Location of the 25 April 2015 **M** 7.8 earthquake (black star) and the 12 May 2015 **M** 7.3 aftershock (white star) and the aftershocks relocated in this study (black dots). The approximate mainshock rupture areas of the 2015 and 1934 earthquakes are also shown (solid and dashed rectangles, respectively). The 2015 rupture area is from Lindsey *et al.* (2015); the 1934 rupture area is approximate, based on the extent of the mapped surface rupture from Sapkota *et al.* (2013) and Bollinger *et al.* (2014). Earthquake locations are current as of 12 June 2015. (b) Intensities from Martin *et al.* (2015) are plotted with the color scale as indicated.

sensors will be combined to develop the Nepal–Shaking Hazard Assessment for Kathmandu and its Environment (N-SHAKE) network. All station information, including information such as station location, sampling rate, and date of installation, is included in Ⓔ Table S1, available in the electronic supplement to this paper.

Complementary to the QCN sensors in Kathmandu is a permanent U.S. Geological Survey (USGS) NetQuakes (network code NQ) strong-motion sensor (NQ.KATNP; Fig. 1b) located at a site in central Nepal, which provides the closest complete recording of the 25 April 2015 **M** 7.8 Gorkha earthquake and early aftershocks. The station began operation in April 2011, but ceased transmission in near real time in 2013 due to an unreliable Internet connection. Initial recordings of the Gorkha sequence were retrieved manually from the ring buffer several days after the mainshock. The lack of Internet connectivity over a period of two years caused the internal clock to drift by 37.381 s. A time correction was applied on 19 May 2015, so that arrival times could be more accurately determined and used to improve locations of the mainshock and early aftershocks. In late May, the USGS Earthquake Disaster Assistance Team replaced the original NQ.KATNP unit with a new NetQuakes instrument, performed a tilt test to confirm the calibration of the original instrument, and confirmed that neither the instrument nor the structure (a well-constructed one-story reinforced concrete building) were disrupted by mainshock shaking. The team then installed the original sensor on the ground floor of NSET headquarters, collocated with an existing QCN sensor (QC.31523). This anchors the N-SHAKE network with two conventional strong-motion (NetQuakes) instruments, including one that will provide direct validation of data recorded by the collocated QCN instrument. Waveforms from the NetQuakes sensors stream data in near real time to the USGS National Earthquake Information Center (NEIC) for earthquake source characterization and are archived and available for download at the Incorporated Research Institutions for Seismology Data Management Center (IRIS-DMC).

In this report, we describe the strong-motion recordings of the 2015 Gorkha **M** 7.8 earthquake and present preliminary results that illustrate the continual potential value and utility of low-cost QCN instruments to improve strong-motion monitoring, particularly in regions where traditional seismic networks are limited.

MAINSHOCK AND LARGE AFTERSHOCK GROUND-MOTION OBSERVATIONS

The 25 April 2015 **M** 7.8 Gorkha earthquake produced strong shaking (European macroseismic scale intensities V–VIII; Martin *et al.*, 2015) that resulted in nearly 9000 fatalities, 23,000 injuries, and thousands of collapsed or seriously damaged buildings (ICIMOD, 2015). This earthquake occurred 81 yrs after the 1934 **M** > 8 Nepal–Bihar earthquake (Sapkota *et al.*, 2013), which resulted in over 15,000 deaths (Rana, 1934; Dunn *et al.*, 1939) and in severe damage in eastern Nepal (Rana, 1934). Based on hazard assessments undertaken, the community of earthquake professionals had long voiced concern about potential losses during a future large earthquake (e.g., Bilham *et al.*, 2001). The 2015 **M** 7.8 Gorkha earthquake initially appeared to be a realization of worst fears, with a somewhat smaller magnitude than the 1934 event, occurring on the plate boundary segment directly beneath the densely populated Kathmandu Valley. Although the Gorkha mainshock took a

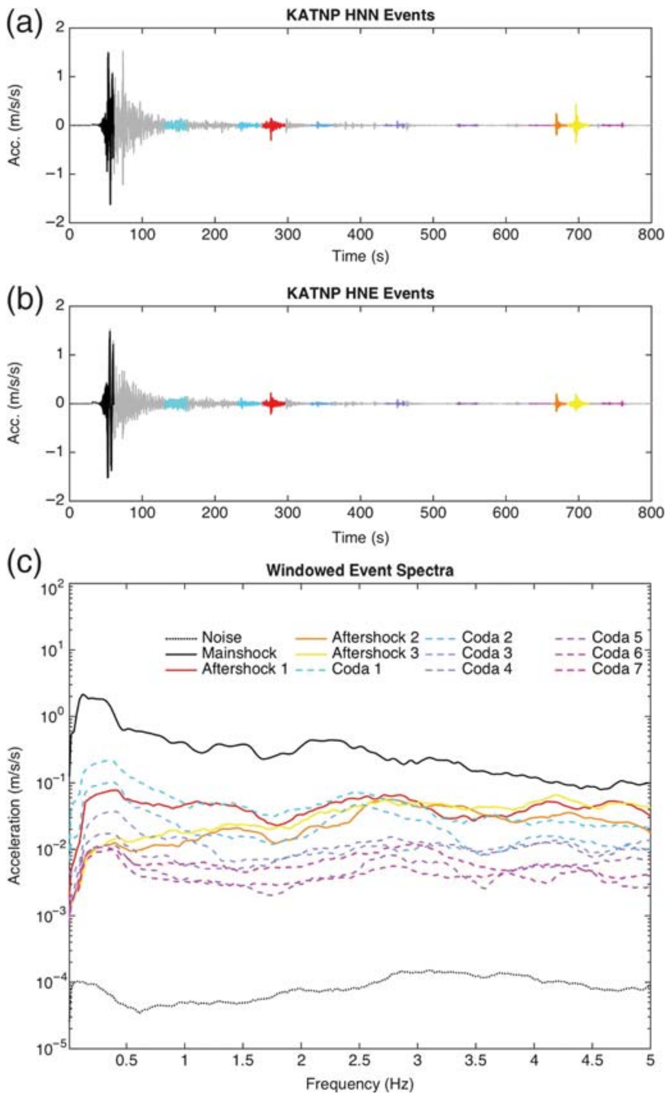

▲ **Figure 2.** Time series of the mainshock and its coda (gray) on (a) the north–south (HNN) and (b) east–west (HNE) components of NQ.KATNP. The coda from the mainshock is visible across the entire ~13 min. record. Time windows used to compute the spectra are indicated by colored segments. Windows are 30 s long and include noise, mainshock, three large aftershocks, and seven coda windows (one every 100 s) following the mainshock. (c) The geometric mean of the horizontal spectra for each of the time windows shown in (a) and (b). The color of each of the time windows is shown in the legend in part (c) and is consistent across all parts of the figure.

heavy toll on property and lives, shaking intensity estimates from Nepal reveal that damage in Kathmandu was lower than would have been predicted given the magnitude and rupture geometry of the earthquake (Martin *et al.*, 2015). The freely available, complete record of the **M** 7.8 Gorkha earthquake from the NetQuakes station NQ.KATNP, which complements a strong-motion recording from an instrument operated by the Nepali Department of Mines and Geology (DMH) (Bhattarai *et al.*, 2015), provides critical quantification of strong ground motions in the Kathmandu Valley (Fig. 2a). This recording indicates that peak ground acceleration (PGA) was surprisingly low, ~16% of *g*. The low PGA value and general character of the waveforms are consistent with the recording from the DMH instrument, confirming the fidelity of both recordings. We first discuss mainshock and aftershock recordings from NQ.KATNP, which we then subsequently use to validate data from the QCN instruments.

In Figure 2b, we show the Fourier amplitude spectra for the mainshock and three early aftershocks, two of which were located by the USGS (**M** 6.1, 06:15:22; **M** 5.1, 06:25:55). To calculate spectra, we remove the mean and trend, apply a 5% cosine taper, and high-pass filter the records above 0.1 Hz. We use windows that begin 5 s before the *P*-wave arrival and end at six times the *S*-wave arrival minus *P*-wave arrival time. The mainshock recording clearly illustrates that initial ground motions were dominated by energy with ≈5 s period. This observed dominant 5 s period does not correspond to the expected natural period of amplification at the NQ.KATNP location in Kathmandu Valley, as inferred from microtremor studies (~2 s; Bhandary *et al.*, 2014), but rather likely reflects the long-period source process of the earthquake (Avouac *et al.*, 2015). The aftershock recordings from NQ.KATNP have peaks at somewhat shorter periods, roughly 4 s (**M** 6.1) and 3 s (**M** 5.4). Additionally, we examine seven 30-s-long windows, one every 100 s, following the mainshock and again see clear resonant energy at 2–4 s period, similar to that seen in the mainshocks and early aftershock records. A strong predominant period close to 2 s is observed during the **M** 7.3 aftershock (Figs. 3 and 4). The absence of the expected weak-motion resonance peak during the mainshock coda, which is generally consistent with observations from the 1994 Northridge, California, sequence (Field *et al.*, 1997), suggests that sediment response was highly and pervasively nonlinear during the mainshock.

In Figure 4, we show the geometric mean of the horizontal acceleration spectra for the mainshock and aftershocks, with magnitudes ranging from **M** 5.6 to 7.3 recorded by both the QCN and NetQuakes NQ.KATNP instruments. We note a good correspondence between spectral amplitudes from QCN versus NQ.KATNP. The recordings from NQ.KATNP reveal more long-period energy. This observation is consistent with expectations; whereas NQ.KATNP is near the center of the valley, QCN–NSET (station QC.31523) and QCN–SNS (station 45298) are located toward the edge of the valley (Fig. 1b), where the expected predominant period of weak motion amplification is 0.6–1 s (Bhandary *et al.*, 2014).

The QCN station QC.31783/01339 is located on the third floor of a building, which allows for preliminary analysis of building response during this earthquake sequence. As expected, data recorded at this site are dominated by structural response, with a strong resonance period at 4–5 Hz. This demonstrates the potential utility of QCN instruments for structural monitoring, although additional work will need to be carried out to verify the accuracy and precision of the instruments and their metadata.

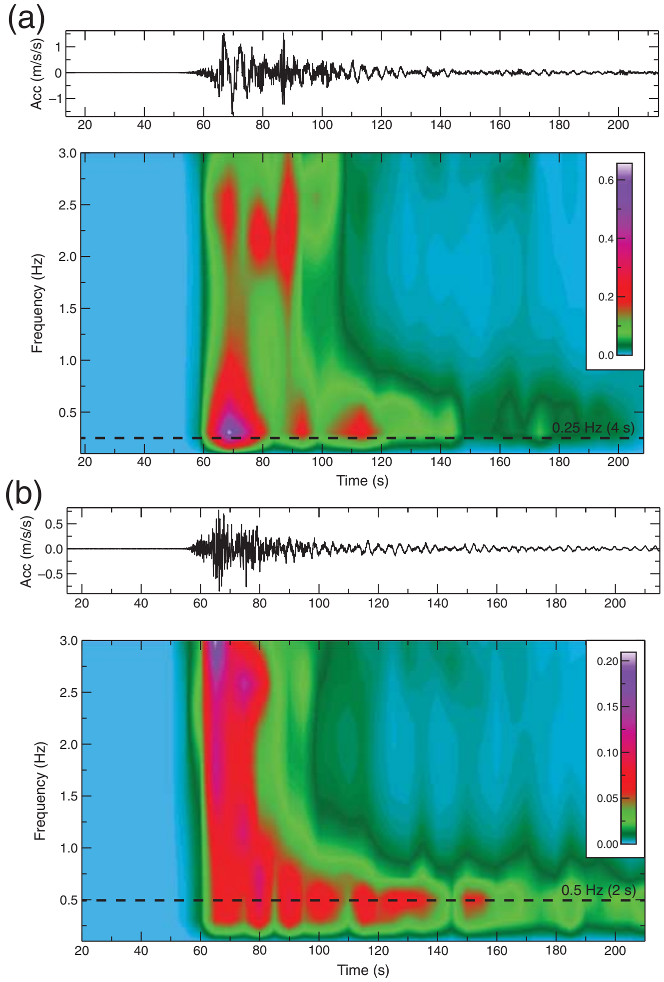

▲ **Figure 3.** Spectrograms for (a) the **M** 7.8 mainshock and (b) the **M** 7.3 aftershock recorded at NQ.KATNP. For both events, spectra are calculated for the north–south component of motion using 10-s-long windows calculated every 5 s. Spectral amplitudes, indicated by color scale, provide indication of relative (square-root) amplitudes.

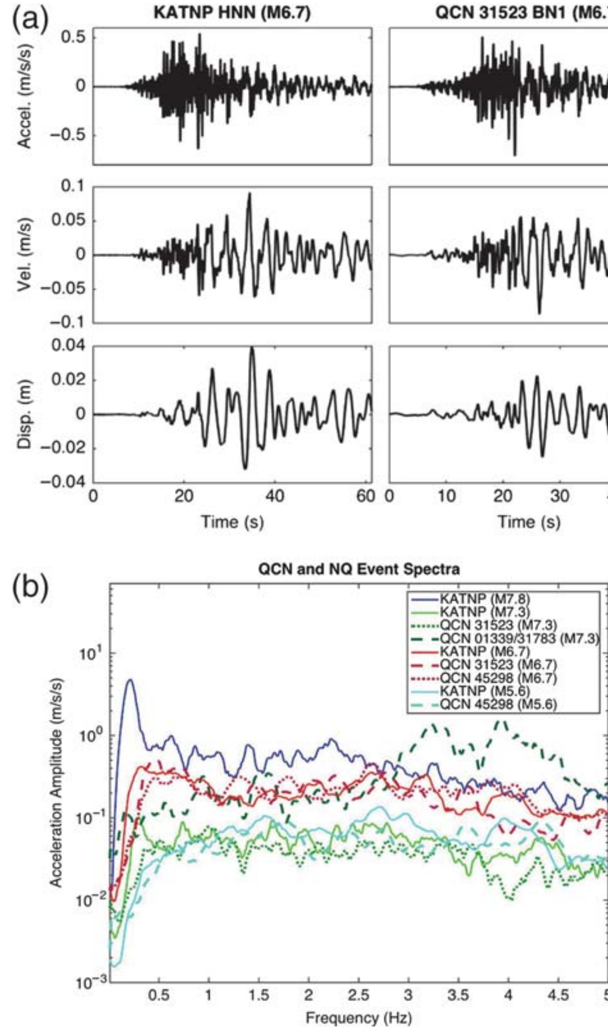

▲ **Figure 4.** (a) North–south (HNN) recording of the **M** 6.7 aftershock (acceleration, velocity, and displacement) on the (left) NetQuakes sensor NQ.KATNP, and (right) by Quake-Catcher Network QCN instrument 31523. (b) Combined geometric mean of the horizontal acceleration spectra for **M** ≥5 earthquakes as recorded on the QCN and NQ.KATNP stations, color coded as shown in the legend.

In addition, for ground-motion analysis, we integrate recordings from the QCN and NQ.KATNP stations to velocity for **M** ≥ 5 earthquakes to examine both PGA and peak ground velocity (PGV) (Fig. 5). A comparison of observed PGA and PGV values to the regional ground-motion prediction equation (GMPE) from Singh *et al.* (1996) confirms the conclusion that the mainshock PGA was surprisingly low. PGA values for **M** 5–7.3 events are also generally lower than predictions from the regional GMPE. PGV values for the larger events are more consistent with predictions; for the mainshock, the PGV value exceeds predictions (Fig. 5).

IMPROVED AFTERSHOCK LOCATIONS

In addition to capturing strong shaking for the **M** 7.8 mainshock and several of the larger aftershocks, the local seismic stations in Kathmandu provide the earliest seismic phase-arrival-time picks available for the earthquake location (Ⓔ Fig. S1). Six different QCN and NetQuakes sensors provided 70 *P*- and *S*-wave arrival-time picks for 33 earthquakes that were used to place constraints on the determination of earthquake source parameters for the entire sequence of 222 earthquakes.

For this study, USGS NEIC single-event hypocenters were relocated using a multiple-event approach based on the hypocentroidal decomposition (HD) algorithm (Jordan and Sverdrup, 1981; McNamara *et al.*, 2015). HD is a multiple-event procedure in the same class of methods that include joint hypocentral determination (Dewey, 1972) and double difference (Waldhauser and Ellsworth, 2000). The HD relocation method takes advantage of correlated travel-time residuals to compute station corrections. HD provides improved hypocenter locations

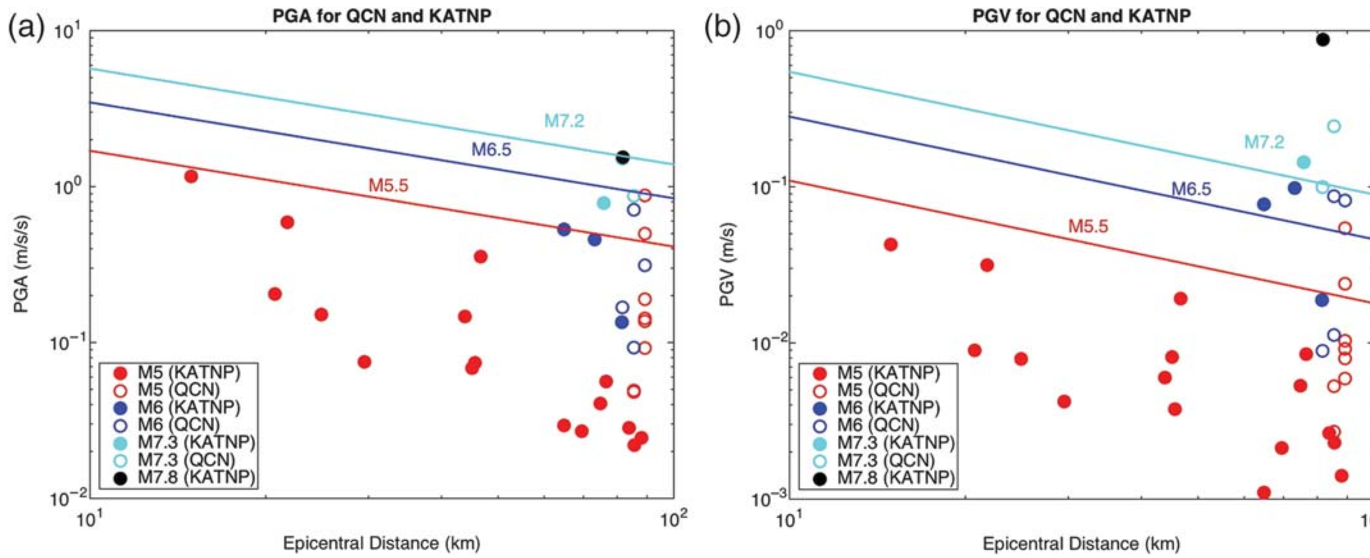

▲ **Figure 5.** (a) The peak ground acceleration (PGA) and (b) peak ground velocity (PGV) values as a function of epicentral distance using the relocated locations determined by this study, as recorded by QCN (open symbols) and KATNP (closed symbols) stations. The color of the symbol represents the magnitude, as identified in the legend. For comparison, we show the ground-motion prediction equations (GMPEs) from Singh *et al.* (1996) for **M** 5.5 (red), 6.5 (blue), and 7.2 (cyan) events. Singh *et al.* (1996) equations are valid up to **M** 7.2; curves for larger magnitudes are not shown.

with minimal location bias and realistic estimates of location uncertainty for each earthquake. Additional constraints include use of a local velocity model (Monsalve *et al.*, 2008) and fixing focal depths for 12 events based on USGS W-phase moment tensor modeling (Hayes *et al.*, 2015). An advantage of the HD method is the ability to relocate a poorly recorded mainshock by tying it to clusters of aftershocks that are recorded by a denser local network.

In this study, we determine relocated hypocenters for a total of 222 earthquakes as shown in Figure 1a and listed in Ⓔ Table S2. The earthquake sequence is most active in the west and east with aftershocks generally bounding the region of maximum slip during the **M** 7.8 mainshock (Hayes *et al.*, 2015). We did not locate all earthquakes observed on local seismic stations, but only those events for which there were a sufficient number of arrival-time observations and good azimuthal coverage to ensure a well-constrained hypocenter. Typically, smaller earthquakes (**M** <4.5) were only recorded on a few stations, making it difficult to determine location and depth accurately. In general, hypocenters shifted a few kilometers to the north from the original NEIC single-event solutions, with uncertainty reduced by a factor of 2 (Ⓔ Fig. S1).

DISCUSSION

In this study, we demonstrate the usefulness of QCN data for ground-motion analyses and aftershock relocations in a region where data access is poor and seismic information is not readily available for dissemination to scientists and the general public. QCN low-cost strong-motion accelerometers provide freely available data from the largest aftershocks of the 25 April 2015 **M** 7.8 Gorkha, Nepal, earthquake, including the **M** 7.3 aftershock on 12 May 2015. In countries where resources are limited, QCN instruments provide a resource to collect seismic data for a fraction of the cost of traditional seismometers.

One of the major advantages of QCN data is the ability to deploy sensors cheaply and rapidly due to the low cost and small size and weight of the sensor. The Gorkha earthquake sequence is yet another example in which conventional Rapid Array Mobilization Procedure deployments could not be mobilized rapidly due to high costs and logistical demands. QCN instruments provide a low-cost alternative that can be quickly and easily shipped in a suitcase without the fear of damage to the sensor in transit. Rapidly deployed QCN instruments can potentially contribute to real-time assessment of aftershock damage and perhaps ultimately to earthquake early warning. QCN RAMP experiments after the **M** 7.1 Darfield, New Zealand, earthquake and the **M** 8.8 Maule, Chile, earthquake have also proven effective for research and education purposes (Chung *et al.*, 2011, 2015; Lawrence *et al.*, 2014) and have provided scientists with a wealth of information to assess ground motion in earthquake prone regions.

Although volunteer-hosted QCN sensors have provided valuable seismic data in regions that are poorly instrumented by conventional networks, there are still challenges to overcome in regard to the Nepal earthquake response. Potential improvements include (1) development of higher-quality sensors with broader frequency and lower noise floor to improve detection of small-magnitude earthquakes and enable modern waveform-modeling methods (we expect MEMS sensors will continue to improve in time, as quality is driven by market forces); (2) establishment of data streaming to seismology community archives and processing centers, including the IRIS-DMC and the USGS NEIC National Strong-Motion Program; and (3) development of backup power systems and use of low-cost microcomputers to obviate the need for a user-supplied laptop or desktop computer.

CONCLUSIONS

Low-cost QCN instrumentation deployed in recent years in the Kathmandu region provided high-quality strong-motion observations of the 25 April 2015 **M** 7.8 Gorkha, Nepal, sequence. Although the mainshock was not fully recorded by QCN instruments due to power failures, one freely available mainshock recording is available from USGS-installed NetQuakes instrument NQ.KATNP. Both NQ.KATNP and QCN instruments installed prior to the mainshock recorded invaluable data for early large aftershocks, including the **M** 7.3 event on 12 May 2015. Data from the conventional strong-motion instrument provide validation for early aftershocks recorded on the QCN instruments. Preliminary results reveal that (1) mainshock PGA was considerably lower than expected; (2) mainshock shaking was strongly peaked at the ∼5 s period, with no evidence of the expected 2 s weak-motion resonance in the central Kathmandu Valley; (3) the predominant periods of large aftershocks, including the **M** 7.3 event on 12 May 2015, were lower than that of the mainshock and more consistent with the expected predominant period of the basin response; and (4) the inclusion of local data significantly improves the aftershock locations determined by the USGS using only regional data. More in-depth analysis will be needed to improve our understanding of near-field ground motions, regional GMPEs, and long-term probabilistic seismic hazard in the region.

Although data from only four near-field strong-motion stations are available for the **M** 7.8 Gorkha earthquake and early aftershock sequence, a project is now underway to develop the N-SHAKE network to improve strong-motion monitoring throughout the Kathmandu Valley, as well as the rest of Nepal. Data from an expanded N-SHAKE network will allow reliable shaking distribution maps to be developed in near real time following future significant earthquakes. As of 12 June 2015, NSET has installed an additional five stations with plans to install an additional 30–40 sensors over the next year. All recorded data, as well as data recorded by NQ.KATNP, will be freely available to the international community in real time.

DATA AND RESOURCES

Data from Quake-Catcher Network (QCN) sensors were available at qcn.stanford.edu (last accessed June 2015); QCN data are now available at qcn.caltech.edu (last accessed July 2015). Data from NQ.KATNP are available from the Center for Engineering Strong Motion Data website at strongmotioncenter.org (last accessed June 2015). This work made use of Generic Mapping Tools, Seismic Analysis Code, and MATLAB software.

ACKNOWLEDGMENTS

We thank the U.S. Geological Survey (USGS) for access to NQ.KATNP data, and Stanford University, which currently hosts the servers that allow Quake-Catcher Network (QCN) data to be transmitted in near real time. In July 2015, the QCN servers moved to Caltech. Incorporated Research Institutions for Seismology (IRIS) and the Southern California Earthquake Center (SCEC) will continue to conduct education and outreach efforts for QCN. We thank Kasey Aderhold, Zhigang Peng, Janet Slate, and three anonymous reviewers for their helpful reviews, which improved the manuscript. We also thank Zhigang Peng for serving as editor. Support for QCN installations and other fieldwork was provided by the U.S. Agency for International Development, Office of Foreign Disaster Assistance. Any use of trade, product, or firm names is for descriptive purposes only and does not imply endorsement by the U.S. Government.

The facilities of IRIS Data Services, and specifically the IRIS Data Management Center, were used for access to waveforms, related metadata, and/or derived products used in this study. IRIS Data Services are funded through the Seismological Facilities for the Advancement of Geoscience and EarthScope (SAGE) Proposal of the National Science Foundation under Cooperative Agreement EAR-1261681.

REFERENCES

Anderson, D. P., and J. Kubiatowicz (2002). The world-wide computer, *Sci. Am.* **286,** 40–47.

Avouac, J.-P., L. Meng, S. Wei, T. Wang, and J.-P. Ampuero (2015). Lower edge of locked Main Himalayan Thurst unzipped by the 2015 Gorkha earthquake, *Nature Geosci.* **8,** 708–711, doi: 10.1038/ngeo2518.

Bhandary, N. P., R. Yatabe, K. Yamamoto, and Y. R. Paudyal (2014). Use of a sparse geo-info database and ambient ground vibration survey in earthquake disaster risk study: A case of Kathmandu Valley, *J. Civ. Eng.* **4,** no. 3A, 20–30, doi: 10.5923/c/jce.201402.02.

Bhattarai, M., L. B. Adhikari, U. P. Gautam, A. Laurendeau, C. Labonne, R. Hoste-Colomer, O. Sebe, and B. Hernandez (2015). Overview of the large April 25th 2015 Gorkha, Nepal, earthquake from accelerometric perspectives, *Seismol. Res. Lett.* **86,** no. 6, doi: 10.1785/0220150140.

Bilham, R., V. K. Gaur, and P. Molnar (2001). Himalayan seismic hazard, *Science* **293,** 1442–1444.

Bollinger, L., S. N. Sapkota, P. Tapponnier, Y. Klinger, M. Rizza, J. Van der Woerd, D. R. Tiwari, R. Pandey, A. Bitri, and S. Bes de Berc (2014). Estimating the return times of great Himalayan earthquakes in eastern Nepal: Evidence from the Patu and Bardibas strands of the Main Frontal Thrust, *J. Geophys. Res. Solid Earth* **119,** doi: 10.1002/2014JB010970.

Chung, A. I., E. S. Cochran, A. E. Kaiser, C. M. Christensen, B. Yildirim, and J. F. Lawrence (2015). Improved rapid magnitude estimation for a community-based, low-cost MEMS accelerometer network, *Bull. Seismol. Soc. Am.* **105,** no. 3, 1314–1323.

Chung, A. I., C. Neighbors, A. Belmonte, M. Miller, H. H. Sepulveda, C. Christensen, R. S. Jakka, E. S. Cochran, and J. F. Lawrence (2011). The Quake-Catcher Network rapid aftershock mobilization program following the 2010 M 8.8 Maule, Chile, earthquake, *Seismol. Res. Lett.* **82,** no. 4, 526–532.

Cochran, E. S., J. F. Lawrence, C. Christensen, and R. S. Jakka (2009). The Quake-Catcher Network: Citizen science expanding seismic horizons, *Seismol. Res. Lett.* **80,** 26–30, doi: 10.1785/gssrl.80.1.26.

Dewey, J. W. (1972). Seismicity and tectonics of western Venezuela, *Bull. Seismol. Soc. Am.* **62,** 1711–1751.

Dunn, J. A., J. B. Auden, A. M. N. Ghosh, S. C. Roy, and D. N. Wadia (1939). The Bihar–Nepal earthquake of 1934, *Memoir. Geol. Surv. India* **73,** 183–391.

Field, E. H., P. A. Johnson, I. A. Beresnev, and Y. Zeng (1997). Nonlinear ground-motion amplification by sediments during the 1994 Northridge earthquake, *Nature* **390,** 599–602.
Hayes, G. P., W. Barnhart, R. Briggs, W. Yeck, D. E. McNamara, D. Wald, J. Nealy, H. Benz, R. Gold, K. Jaiswal, *et al.* (2015). Rapid characterization of the 2015 M_w 7.8 Nepal (Gorkha) earthquake, *Seismol. Res. Lett.* **86,** no. 6, doi: 10.1785/0220150145.
ICIMOD (2015). Nepal Earthquake 2015, http://www.icimod.org/?q=17851 (last accessed June 2015).
Jordan, T. H., and K. A. Sverdrup (1981). Teleseismic location techniques and their application to earthquake clusters in the south-central Pacific, *Bull. Seismol. Soc. Am.* **71,** 1105–1130.
Lawrence, J. F., E. S. Cochran, A. Chung, A. Kaiser, C. M. Christensen, R. Allen, and M. Taufer (2014). Rapid earthquake characterization using MEMS accelerometers and volunteer hosts following the M 7.2 Darfield, New Zealand, earthquake, *Bull. Seismol. Soc. Am.* **104,** no. 1, 184–192.
Lindsey, E. O., R. Natsuaki, X. Xu, M. Shimada, M. Hashimoto, D. Melgar, and D. T. Sandwell (2015). Line of sight displacement from ALOS-2 Interferometry: M 7.8 Gorkha earthquake and M 7.3 aftershock, *Geophys. Res. Lett.*, doi: 10.1002/2015GL065385.
Martin, S. S., S. E. Hough, R. Bilham, and C. Hung (2015). Ground motions from the 2015 M_w 7.8 Gorkha, Nepal, earthquake, constrained by a detailed assessment of macroseismic data, *Seismol. Res. Lett.* **86,** no. 6, doi: 10.1785/0220150138.
McNamara, D. E., H. M. Benz, R. B. Herrmann, E. A. Bergman, P. Earle, A. Holland, R. Baldwin, and A. Gassner (2015). Earthquake hypocenters and focal mechanisms in central Oklahoma reveal a complex system of reactivated subsurface strike-slip faulting, *Geophys. Res. Lett.* **42,** 2742–2749, doi: 10.1002/2014GL062730.
Monsalve, G., A. Sheehan, C. Rowe, and S. Rajaure (2008). Seismic structure of the crust and the upper mantle beneath the Himalayas: Evidence for eclogitization of lower crustal rocks in the Indian plate, *J. Geophys. Res.* **113,** no. B08315, doi: 10.1029/2007JB005424.
Nobuo, T., K. Sawada, M. Shigefuji, S. M. Bijukchhen, M. Ichiyanagi, T. Sasatain, Y. P. Dhakal, S. Rajaure, and M. R. Dhital (2015). Shallow underground structure of strong ground motion observation sites in the Kathmandu Valley, *J. Nepal Geol. Soc.* **48,** 40.
Rana, B. S. J. B. (1934). *Nepalko mahabhukamp*, English translation by Kesar Lal (2013) (Editor), Ratna Pustak Bhandar, Kathmandu, Nepal (in Nepali).
Sapkota, S. N., L. Bollinger, Y. Killinger, P. Tapponier, Y. Gaudemer, and D. Tiwari (2013). Primary surface ruptures of the great Himalayan earthquakes in 1934 and 1255, *Nat. Geosci.* **6,** 71–76, doi: 10.1038/ngeo1669.
Singh, R. P., A. Aman, and Y. J. J. Prasad (1996). Attenuation relations for strong seismic ground motion in the Himalayan region, *Pure Appl. Geophys.* **147,** no. 1, 161–180.
Waldhauser, F., and W. L. Ellsworth (2000). A double-difference earthquake location algorithm: Method and application to the northern Hayward fault, California, *Bull. Seismol. Soc. Am.* **90,** 1353–1368.

Amod Mani Dixit
Surya Narayan Shrestha
Sudhir Rajaure
National Society for Earthquake Technology–Nepal
Sainbu Residential Area
Ward 4, Bhaisepati, Lalitpur District
GPO Box 13775
Kathmandu, Nepal

Adam T. Ringler
U.S. Geological Survey
Albuquerque Seismological Laboratory
P.O. Box 82010
Albuquerque, New Mexico 87198 U.S.A.
aringler@usgs.gov

Danielle F. Sumy
Incorporated Research Institutions for Seismology
1200 New York Avenue
Suite 400
Washington, D.C. 20005 U.S.A.

Elizabeth S. Cochran
Susan E. Hough
U.S. Geological Survey
525 S. Wilson Avenue
Pasadena, California 91106 U.S.A.

Stacey S. Martin
Earth Observatory of Singapore (EOS)
Nanyang Technological University
Singapore 639798

Steven Gibbons
NORSAR
PO Box 53
2027 Kjeller, Norway

James H. Luetgert
U.S. Geological Survey
345 Middlefield Road
MS 977
Menlo Park, California 94025 U.S.A.

John Galetzka
UNAVCO
6350 Nautilus Drive
Boulder, Colorado 80301 U.S.A.

Daniel E. McNamara
U.S. Geological Survey
National Earthquake Information Center
1711 Illinois Street
Golden, Colorado 80401 U.S.A.